

Spectroscopy and Crystal-Field Analysis of Low-Symmetry Er^{3+} Centres in K_2YF_5 Microparticles

Pratik S. Solanki^{a,b}, Michael F. Reid^{a,b,*} and Jon-Paul R. Wells^{a,b,*}

^aThe School of Physical and Chemical Sciences, University of Canterbury, PB4800 Christchurch 8140, New Zealand,

^bThe Dodd-Walls Centre for Photonic and Quantum Technologies, New Zealand,

ARTICLE INFO

Keywords:

rare-earth
crystal-field analysis
spectroscopy
Erbium
 K_2YF_5

ABSTRACT

K_2YF_5 crystals doped with lanthanide ions have a variety of possible optical applications. Owing to the low symmetry of the system, the crystal structure cannot be unambiguously determined by x-ray diffraction. However, electron-paramagnetic resonance studies have demonstrated that lanthanide ions substitute for yttrium in sites of C_s local symmetry. In this work, we use high-resolution absorption and laser spectroscopy to determine electronic energy levels for Er^{3+} ions in K_2YF_5 microparticles. A total of 39 crystal-field energy levels, distributed among 7 multiplets of the Er^{3+} ion, have been assigned. This optical data is used for crystal-field modelling of the electronic structure of Er^{3+} in K_2YF_5 . Our model is fitted not only to the electronic energy levels, but also to the ground-state g-tensor. This magnetic-splitting data defines the axis system of the calculation, avoiding ambiguities associated with low-symmetry crystal-field fits.

1. Introduction

Lanthanide ion doped potassium yttrium pentafluoride crystals (K_2YF_5) are promising optically active media that have been investigated for a variety of applications, including phosphors, thermoluminescence dosimeters, laser crystals, and passive Q-switching [1, 2, 3, 4, 5]. An understanding of the electronic structure of lanthanide ions in this host requires a knowledge of the crystal structure. X-ray diffraction is unable to distinguish between two possible space groups, $Pnam$ and $Pna2_1$. However, electron paramagnetic resonance (EPR) studies indicate that the structure is monoclinic, with space group $Pnam$ [6, 7]. The unit cell dimensions are $a = 10.820 \text{ \AA}$, $b = 6.613 \text{ \AA}$, $c = 7.249 \text{ \AA}$. Each Y^{3+} ion is surrounded by seven fluoride ions with C_s point group symmetry. The YF_7 polyhedra form chains parallel to the c-axis. The distance between the intra-chain Y^{3+} - Y^{3+} ions is around 3.7 \AA , whereas the shortest inter-chain separation is $\sim 5 \text{ \AA}$. As with other fluoride hosts, K_2YF_5 has a *relatively* low Debye temperature and therefore band phonon cutoff frequency of around 480 cm^{-1} [8, 9].

EPR has been used to investigate the ground state magnetic splittings for Ce^{3+} , Gd^{3+} [6], Er^{3+} , and Yb^{3+} [7]. Optical spectroscopy has been performed, with varying degrees of depth and rigour,

*Corresponding authors

✉ mike.reid@canterbury.ac.nz (M.F. Reid); jon-paul.wells@canterbury.ac.nz (J.R. Wells)
ORCID(s): 0000-0002-2984-9951 (M.F. Reid); 0000-0002-8421-6604 (J.R. Wells)

1

on K₂YF₅ bulk single crystals doped with Pr³⁺ [10, 11], Nd³⁺ [12, 13], Sm³⁺ [3], Eu³⁺ [14], Tb³⁺ [15, 9], Er³⁺ [16, 8, 17, 18] and Tm³⁺ [19, 20].

Magnetic-splitting data has been shown to be crucial for crystal-field calculations in low-symmetry systems [21, 22, 23, 24]. In those studies, directional information such as EPR-derived ground-state *g*-tensors and/or rotational Zeeman data were used to give a unique orientation for the axis system used in the calculations. In high symmetries, the crystal-field parameters may be uniquely determined once an axis system is chosen. For example, in O_h symmetry the four-fold axis may be chosen to be along *x*, *y*, and *z*. In that case, the two (real) crystal-field parameters be unambiguously determined. In low symmetries it is no longer possible to unambiguously determine crystal-field parameters by fitting to electronic energy levels. In the case of C₁ (i.e. no) symmetry, parameters fitted to only electronic energies may be rotated arbitrarily in three dimensions, changing both the *phases* and the *magnitudes* of the parameters [25]. For C_s symmetry, relevant for K₂YF₅, the *z* axis may be chosen perpendicular to the mirror plane. However, any rotation about *z* leaves the electronic energies invariant and such a rotation changes the *phases* of the complex parameters.

Karbowiak *et al.* [12] reported a comprehensive analysis of electronic energy levels of Nd³⁺ in K₂YF₅. Their crystal-field fit used C_s symmetry and the starting parameters were based on the superposition model. Unfortunately, there is no magnetic-splitting data available for that system, so the orientation of calculated magnetic moments can not be checked against experiment.

EPR data is available for Er³⁺-doped K₂YF₅ [7]. In this paper, we present detailed spectroscopic studies of K₂YF₅ microparticles doped with 2 mol% of Er³⁺, prepared by the solvothermal method. Powder X-ray diffraction (PXRD) and scanning electron microscopy (SEM) were used to obtain information about the crystallinity and morphology of these microcrystals. The 2 mol% doping was chosen to give a good signal in both absorption and emission. A very high concentration can quench luminescence due to cross-relaxation. A detailed energy-level scheme has been deduced from high-resolution absorption and laser excited fluorescence for samples nominally cooled to 10 K. This experimental data, supplemented by EPR data, is used to fit a crystal-field model using techniques that build upon our earlier work on C₁ sites in Y₂SiO₅ [22, 23, 24].

2. Materials and Methods

2.1. Materials

Yttrium nitrate (Y(NO₃)₃, 99.90%) and erbium nitrate pentahydrate (Er(NO₃)₃ · 5H₂O, 99.90%) obtained from Sigma-Aldrich (St. Louis, USA) were used as a rare earth ion source. Anhydrous potassium fluoride (KF, BDH laboratory, 98.00%) and potassium hydroxide (KOH, Sigma-Aldrich, 99.00%) were used as the fluoride source. All the chemicals were used as received. Milli-Q water, ethanol (analytical grade, 99.50%), and Oleic acid (analytical grade, 99.50%), were employed to wash and prepare the samples.

2.2. Synthesis of K₂YF₅:Er³⁺ microparticles

K₂YF₅ microparticles doped with two mol% Er³⁺ were synthesized via the solvothermal method [26, 27]. The appropriate amounts of KOH (35 mmol) were dissolved in 7.5 ml deionized water in a beaker. After that, 25 ml ethanol and 25 ml oleic acid were added. Then a 10 mL aqueous solution containing 80 mmol of KF was added to the above solution and stirred to make a uniform solution. Lastly, 10 ml of Y(NO₃)₃ (1.98 mmol) and Er(NO₃)₃ · 5H₂O (0.02 mmol) aqueous solution was

added to the above-mixed solution. After stirring for 30 minutes, the as-obtained milky solution was transferred into a 100 mL of Teflon-lined stainless-steel autoclave and then heated at 220°C for 24 h. After that, the autoclave cooled naturally to room temperature, and the precipitate was collected through centrifugation (7000 rpm, 10 minutes), thoroughly washed with ethanol, and then dried at 80°C for 12 h.

2.3. Characterisation and Spectroscopy

Powder X-ray diffraction patterns were collected on a RIGAKU 3 kW SmartLab X-ray diffractometer employing a CuK α 1 radiation source, $\lambda=1.5406$ Å. Scanning electron microscope (SEM) images were obtained with a JEOL 7000F scanning electron microscope operating at 15 kV.

The absorption measurements were carried out using an N₂ purged Bruker Vertex 80 FTIR with a resolution of 0.075 cm⁻¹. The powder was pressed into thin pellets using a pellet maker and then placed into a copper sample holder, which itself was in thermal contact with the cold finger of a closed cycle cryostat, for absorption measurements. In order to perform fluorescence spectroscopy, a pulsed N₂ laser pumped PTI GL-302 dye laser was employed as the excitation source, providing wavelength tunability through the visible region. The detection system consisted of a Horiba iHR550 monochromator equipped with either a Hamamatsu R2257P thermoelectrically cooled visible photomultiplier tube (PMT) or a thermoelectrically cooled Hamamatsu H10330C near-infrared PMT. For both absorption and fluorescence measurements a Janis CCS-150 closed-cycle cryostat cooled the sample to 10 K.

2.4. Crystal-Field Calculations

In our calculations, the 4f¹¹ configuration of Er³⁺ is modelled by a parametrized Hamiltonian [28, 29, 30]:

$$H = H_{\text{FI}} + H_{\text{CF}} + H_{\text{Z}} \quad (1)$$

H_{FI} is the free ion contribution, H_{CF} is the crystal-field contribution, and H_{Z} is the Zeeman interaction. The crystal-field contribution is expanded in terms of spherical tensors as:

$$H_{\text{CF}} = \sum_{k,q} B_q^k C_q^{(k)}. \quad (2)$$

The B_q^k are crystal-field parameters and the $C_q^{(k)}$ are Racah spherical tensor operators acting within the 4f^N configuration. In this Hamiltonian, k is restricted to 2, 4, and 6. In C_s symmetry parameters with odd q are zero, but the parameters with $q \neq 0$ are complex. The Zeeman interaction may be written as:

$$H_{\text{Z}} = \mathbf{B} \cdot (\mathbf{L} + g_s \mathbf{S}), \quad (3)$$

where \mathbf{B} is the (externally applied) magnetic field, \mathbf{L} and \mathbf{S} are orbital and spin angular momentum operators and g_s the g-value of the electron.

Fitting crystal-field parameters for low-symmetry systems is challenging. Our previous work on C₁ sites in Y₂SiO₅ [22, 23, 24] has shown that the addition of magnetic-splitting data is essential to fix the orientation of the axis system. For this work, we chose the x , y and z axes to be along the a , b , and c crystallographic axes. The mirror plane is, therefore, perpendicular to the z axis.

3. Results and Discussion

3.1. Phase, Morphology, and Composition

Phase identification of the $\text{K}_2\text{YF}_5: 2\text{mol}\%\text{Er}^{3+}$ microparticles was performed using the PXRD technique. As shown in Figures 1 (a) and (b), the PXRD patterns of the as synthesised $\text{K}_2\text{YF}_5:\text{Er}$ microparticles are plotted against the orthorhombic K_2YF_5 crystal data (JCPDS No. 72-2387) for comparison [26, 27]. The diffraction peaks of the samples are in good agreement with the reference data for orthorhombic K_2YF_5 (space group Pna21). To further investigate the morphology of the $\text{K}_2\text{YF}_5:\text{Er}$ microparticles, scanning electron microscopy (SEM) was used. Figure 1 (c) shows that the $\text{K}_2\text{YF}_5:\text{Er}$ sample is a mixture of hexagonal and octagonal microcrystals with a particle size distribution ranging from 4 μm to 14 μm .

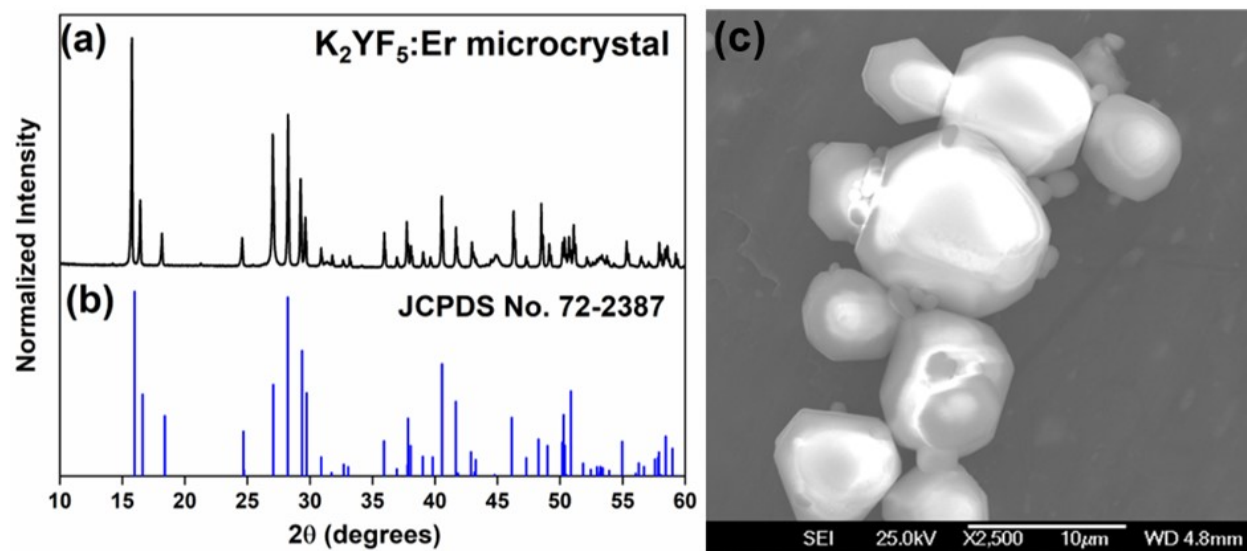


Figure 1: Powder X-ray diffraction patterns of (a) the $\text{K}_2\text{YF}_5:\text{Er}$ microcrystals and (b) the standard orthorhombic K_2YF_5 (JCPDS. No. 72-2387) reference pattern. (c) SEM image of the $\text{K}_2\text{YF}_5:\text{Er}$ microcrystals.

3.2. Optical Absorption and Fluorescence Spectra

Figure 2 shows absorption spectra of the pelletized K₂YF₅:2%Er³⁺ microparticle ensembles for transitions between the ⁴I_{15/2} ground multiplet and the ⁴I_{13/2}, ⁴I_{11/2}, ⁴I_{9/2}, ⁴F_{9/2}, ⁴S_{3/2} and ²H_{11/2} multiplets with samples cooled to a nominal temperature of 10 K. Numerical labels are used to indicate assignments to the initial and final states within the ground and excited multiplets. Due to the approximately 10 micron diameter of these particles, the particle size distribution does not play a substantial role in determining the measured inhomogeneous linewidths which are not significantly greater than those observed in bulk crystals [18]. One of the notable features of the spectra is the observation of transitions from thermally populated excited states within the ground multiplet. This occurs due to the difficulty in getting good thermal contact across the entire pellet with the copper sample mount. Due to the fact that even within a pelletized sample, there are limited contact points from particle to particle, the only way to fully overcome this would be to immerse the entire pellet in liquid helium. However the observation of additional transitions is, in fact, an advantage here since the purpose is to assign energy levels. All of the experimentally assigned energy levels are given in Table 1.

Fluorescence spectra were recorded throughout the visible and near infrared regions with the microparticle sample excited at 19157 cm⁻¹, corresponding to the ⁴I_{15/2}Z₁ → ²H_{11/2}F₁ transition. The nominal base temperature for the sample was recorded as 10 K. Figure 3 shows the downshifted fluorescence of the ⁴I_{13/2}, ⁴I_{11/2}, ⁴I_{9/2}, ⁴F_{9/2}, and ⁴S_{3/2} multiplets to the ground ⁴I_{15/2} multiplet. As is expected for Er³⁺, transitions emanating from the ⁴I_{13/2} multiplet are amongst the strongest (and magnetic dipole allowed) whilst those from the ⁴I_{9/2} multiplet are weak due to the small energy gap to the ⁴I_{11/2} multiplet which allows for significant non-radiative depopulation. As with the absorption spectra, numerous transitions from thermally populated excited state levels can be observed for transitions from any given multiplet. The complete list of assigned crystal-field levels is presented in Table 1.

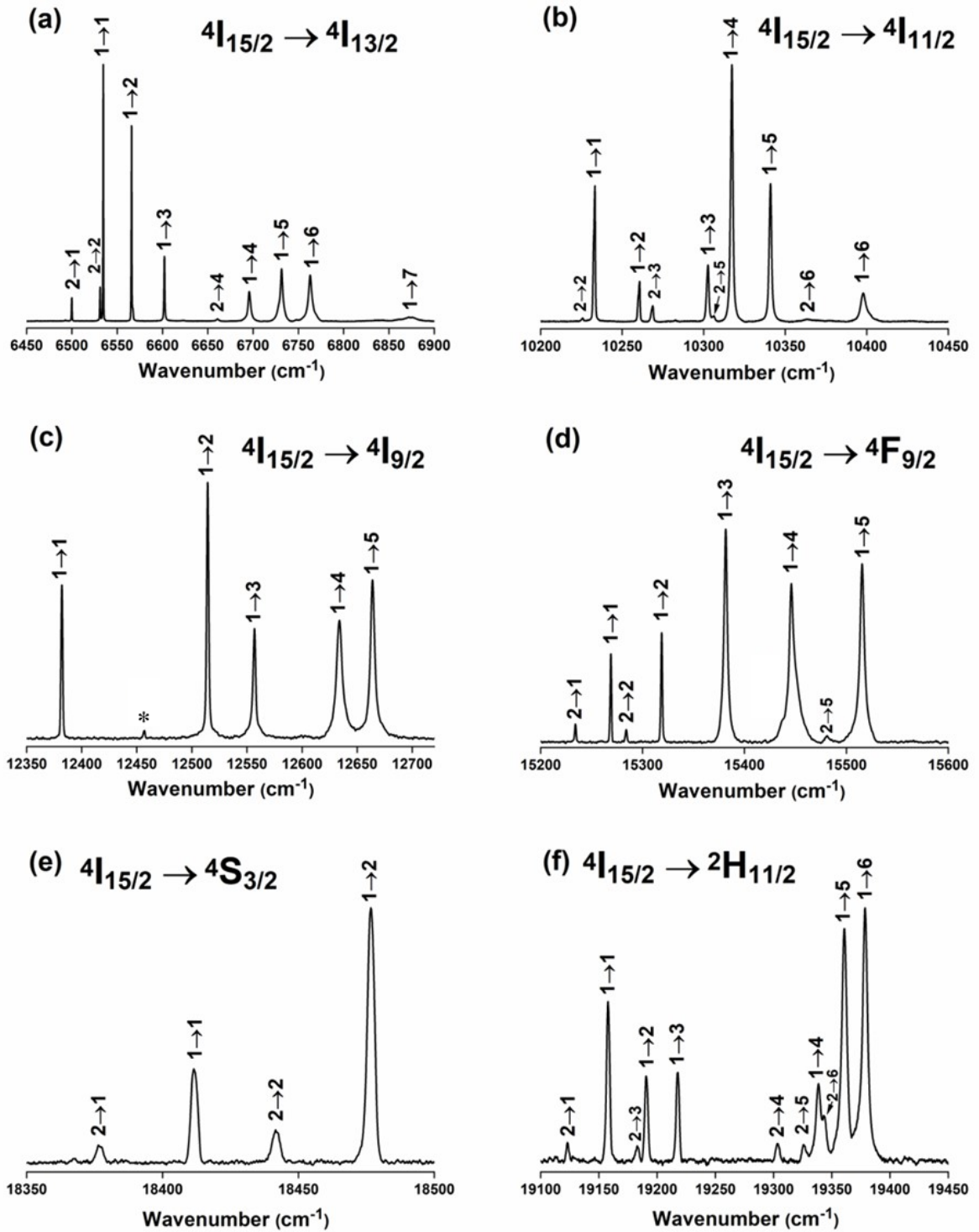


Figure 2: 10 K absorption spectra for the (a) $4I_{15/2} \rightarrow 4I_{13/2}$; (b) $4I_{15/2} \rightarrow 4I_{11/2}$; (c) $4I_{15/2} \rightarrow 4I_{9/2}$; (d) $4I_{15/2} \rightarrow 4F_{9/2}$; (e) $4I_{15/2} \rightarrow 4S_{3/2}$; (f) $4I_{15/2} \rightarrow 2H_{11/2}$ transitions of Er^{3+} doped K_2YF_5 microcrystals. The transition labelled with an asterisk is unassigned.

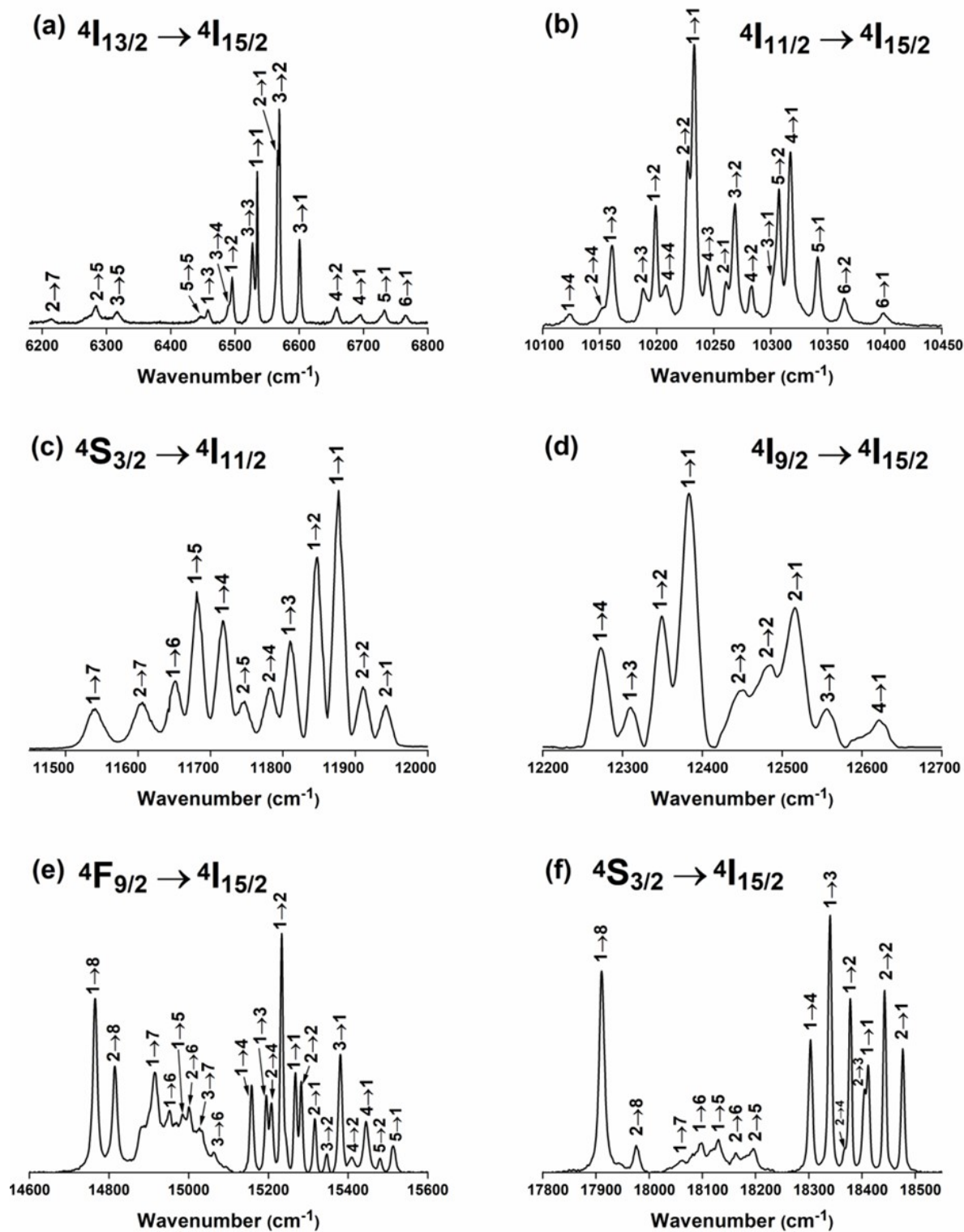


Figure 3: 10 K fluorescence spectra of Er³⁺ doped K₂YF₅ microcrystals excited at 19157 cm⁻¹ for the transitions: (a) $4I_{13/2} \rightarrow 4I_{15/2}$; (b) $4I_{11/2} \rightarrow 4I_{15/2}$; (c) $4I_{9/2} \rightarrow 4I_{15/2}$; (d) $4F_{9/2} \rightarrow 4I_{15/2}$; (e) $4S_{3/2} \rightarrow 4I_{15/2}$; (f) $2H_{11/2} \rightarrow 4I_{15/2}$. The transitions in (c) and (d) were relatively weak, so the scans were taken with larger slit settings and wavelength steps.

3.3. Crystal-Field Analysis

The parameters in our crystal-field model are fitted to both the electronic energy levels (Table 1) and the ground-state *g*-tensor (Table 2). In our calculation, the *x*, *y*, and *z* axes correspond to the crystallographic *a*, *b* and *c* axes. As discussed above, the Y³⁺ sites that the Er³⁺ ions substitute into have C_s symmetry, with the mirror plane being the *x*-*y* plane [6]. The sites have several distinct orientations, related by rotations or reflections, but there are only two sets of magnetically-inequivalent sites [6, 7], with different *g*-tensors, as indicated in Table 2. The crystal-field Hamiltonian for the two sets of sites are related by a complex conjugation of the crystal-field parameters.

The fitting approach followed Ref. [22]. Calculations of zero-field electronic energy levels were carried out in parallel to calculations for 12 orientations of the magnetic field. The weighted χ^2 used in the minimization process consisted of squares of differences between the calculated and experimental electronic energies and squares of differences between the ground-state magnetic splittings and splittings calculated from the *g*-tensor. The magnetic splittings were weighted more heavily than the electronic energies. A basin-hopping algorithm was used to search the parameter space. We allowed the Coulomb, F^k , spin-orbit, ζ , and crystal-field, B_q^k , parameters to vary freely. Other parameters were fixed at the fitted values reported by Carnall *et al.* for Er³⁺ in LaF₃ [28]. An intermediate-coupled basis set was used, truncated at 30,000 cm⁻¹ (15 *J* multiplets), to speed up the calculation.

Table 3 gives fitted parameters for Nd³⁺ in K₂YF₅ [12] and for two different fits for Er³⁺ in K₂YF₅. Fit A was obtained by using the Nd³⁺ parameters as a starting point. This gave a good fit but we also searched for a global minimum by trying other starting points. The best fit we obtained is presented as Fit B. Uncertainties for this fit were estimated using the Monte-Carlo approach described in Ref. [22] and the predicted energy levels for these parameters are given in Table 1. For both fits the calculated *g*-tensor agrees with the experimental data (Table 2) to the accuracy of the measurements. For Fit A, the signs of B_0^2 , B_0^4 , and B_0^6 are the same as for Nd³⁺. Note that since the Nd³⁺ fit did not include any magnetic splitting data, the overall phase of the complex parameters is undetermined. Fit B is quite different, with opposite signs from the Nd³⁺ fit for B_0^4 and B_0^6 .

Karbowiak *et al.* [12] used the superposition model to investigate the relationship between the Nd³⁺ crystal-field parameters and the geometry of the site. In the superposition-model calculations, they assumed the *Pna*2₁ space group and therefore C₁ site symmetry, whereas the EPR results of Refs. [6, 7] are consistent with the *Pnam* space group and C_s site symmetry. However, the geometry they determined had approximate C_s symmetry and that symmetry was used in their crystal-field calculation. Their calculation (Table 5 of [12]) predicts a positive B_0^2 , a positive B_0^4 , and a negative B_0^6 . Their Nd³⁺ fit gives a negative B_0^2 , a positive B_0^4 , and a negative B_0^6 . However, as they point out, the $k = 2$ parameters are expected to be more sensitive to long-range electrostatic contributions than the $k = 4$ and $k = 6$ parameters. Our best fit (Fit B) has opposite signs to the superposition-model prediction for all three of B_0^2 , B_0^4 , and B_0^6 , whereas our Fit A, like the Nd³⁺ fit, is in agreement for B_0^4 and B_0^6 . Our energy-level data set is relatively small, so it is possible that the inclusion of more energy-level or magnetic-splitting data would result in a global minimum in better agreement with the superposition model.

Spectroscopy of Er³⁺ in K₂YF₅**Table 1**

Experimental and fitted electronic energy levels for Er³⁺ doped K₂YF₅ microcrystals. All energies are in cm⁻¹. The experimentally determined energy levels have an associated uncertainty of 1 cm⁻¹. The calculated levels are from the Fit B parameter set of Table 3. The alphanumeric labels follow the convention of Dieke [31].

Multiplet	State	Measured	Fit
⁴ I _{15/2}	Z ₁	0	-2
	Z ₂	35	41
	Z ₃	74	77
	Z ₄	111	111
	Z ₅	283	279
	Z ₆	314	314
	Z ₇	349	357
	Z ₈	502	489
⁴ I _{13/2}	Y ₁	6534	6539
	Y ₂	6566	6568
	Y ₃	6601	6602
	Y ₄	6695	6697
	Y ₅	6731	6739
	Y ₆	6763	6761
	Y ₇	6873	6873
⁴ I _{11/2}	A ₁	10233	10222
	A ₂	10260	10250
	A ₃	10302	10297
	A ₄	10317	10316
	A ₅	10340	10341
	A ₆	10397	10407
⁴ I _{9/2}	B ₁	12382	12380
	B ₂	12514	12506
	B ₃	12556	12559
	B ₄	12633	12626
	B ₅	12664	12677
⁴ I _{9/2}	D ₁	15268	15272
	D ₂	15318	15313
	D ₃	15381	15377
	D ₄	15445	15446
	D ₅	15515	15522
⁴ S _{3/2}	E ₁	18411	18403
	E ₂	18476	18476
² H _{11/2}	F ₁	19157	19166
	F ₂	19190	19199
	F ₃	19217	19213
	F ₄	19338	19333
	F ₅	19360	19363
	F ₆	19378	19375

Table 2

Experimental ground-state g-tensors for the two magnetically-inequivalent sites in Er³⁺ doped K₂YF₅ in the crystal axis system ($x = a$, $y = b$, $z = c$). Principal values from Ref. [7] are $g_x = 0.81$, $g_y = 13.6$, $g_z = 3.19$, with z along the crystal c axis and x and y in the a - b plane with x rotated from a by an angle of $\pm 87.6^\circ$.

g_{xx}	g_{xy}	g_{xz}	g_{yy}	g_{yz}	g_{zz}
13.59	∓ 0.54	0	0.83	0	3.19

Table 3

Crystal-field parameters for Nd³⁺ and Er³⁺ doped K₂YF₅ in units of cm⁻¹. In Fit A and Fit B the free-ion parameters not given in the Table were fixed to the values obtained for Er³⁺ doped LaF₃ [28]. The Nd³⁺ parameters are from Ref. [12]. Fit A was obtained by using the Nd³⁺ parameters as a starting point. Fit B was the best fit obtained from a global search. Weighted χ^2 for the Fit A and Fit B were 5.39 and 4.37 respectively.

Parameter	Nd ³⁺ [12]	Er ³⁺ Fit A	Er ³⁺ Fit B	Uncertainty
E_{avg}		35631	35630	27
F^2		96310	96290	35
F^4		68451	68479	45
F^6		53383	53371	19
ζ		2361	2361	16
B_0^2	-585	-256	-379	43
B_2^2	$322 - 63i$	$-348 - 195i$	$-89 - 408i$	$47 + 62i$
B_0^4	77	792	-1267	14
B_2^4	$-1069 + 1167i$	$1220 + 580i$	$-72 - 65i$	$34 + 40i$
B_4^4	$353 - 108i$	$143 - 666i$	$-1294 - 142i$	$31 + 21i$
B_0^6	-521	-544	270	15
B_2^6	$197 + 19i$	$41 - 75i$	$134 - 85i$	$42 + 18i$
B_4^6	$-428 - 492$	$-5 + 162i$	$-340 - 102i$	$24 + 31i$
B_6^6	$385 - 470i$	$-284 + 18i$	$-192 + 186i$	$27 + 40i$

4. Conclusions

We have presented detailed optical spectroscopy of Er³⁺ in K₂YF₅ microcrystals and deduced energy levels up to 20,000 cm⁻¹. The optical data has been combined with EPR data for the magnetic splitting of the ground state to obtain a crystal-field fit with a known axis orientation. Crystal-field modelling provides a powerful tool to understand the electronic structure of lanthanide ions in crystal hosts and hence to optimise applications. We have shown that in low-symmetry hosts the addition of magnetic measurements provides crucial information for such modelling.

CRedit authorship contribution statement

Pratik S. Solanki: Investigation, Formal analysis, Writing - original draft. **Michael F. Reid:** Conceptualization, Software, Investigation, Supervision, Writing - review and editing. **Jon-Paul R. Wells:** Supervision, Writing - review and editing, Visualization, Resources, Funding Acquisition, Project Administration.

References

- [1] HW Kui, D Lo, YC Tsang, NM Khaidukov, and VN Makhov. Thermoluminescence properties of double potassium yttrium fluorides singly doped with Ce³⁺, Tb³⁺, Dy³⁺ and Tm³⁺ in response to α and β irradiation. *Journal of Luminescence*, 117(1):29–38, 2006.
- [2] Luiz Oliveira de Faria, D Lo, HW Kui, NM Khaidukov, and Maria do Socorro Nogueira. Thermoluminescence response of K₂YF₅: Tb³⁺ crystals to photon radiation fields. *Radiation Protection Dosimetry*, 112(3):435–438, 2004.
- [3] NM Khaidukov, Vu Xuan Quang, Ung Thi Dieu Thuy, Luong Duy Thanh, Vu Phi Tuyen, Nguyen Xuan Ca, and Phan Van Do. Study on optical properties and upconversion luminescence of K₂YF₅: Sm³⁺ single crystals. *Journal of Luminescence*, 237:118201, 2021.
- [4] X Wang, G De, and Y Liu. Synthesis of orthorhombic K₂YF₅:Yb³⁺, Er³⁺/Tm³⁺ nanocrystals and highly efficient multicolor up-conversion luminescence. *Materials Research Bulletin*, 110:181–189, 2019.
- [5] P.A. Loiko, E.V. Vilejshikova, N.M. Khaidukov, M.N. Brekhovskikh, X. Mateos, M. Aguiló, and K.V. Yumashev. Judd–Ofelt modeling, stimulated-emission cross-sections and non-radiative relaxation in Er³⁺:K₂YF₅ crystals. *Journal of Luminescence*, 180:103–110, December 2016.
- [6] F Lonck, D Zverev, H Vrielinck, NM Khaidukov, and F Callens. K₂YF₅ crystal structure determined by using rare-earth ions as paramagnetic probes. *Physical Review B*, 75(14):144427, 2007.
- [7] DG Zverev, H Vrielinck, E Goovaerts, and F Callens. Electron paramagnetic resonance study of rare-earth related centres in K₂YF₅: Tb³⁺ thermoluminescence phosphors. *Optical Materials*, 33(6):865–871, 2011.
- [8] D Wang, M Yin, S Xia, VN Makhov, NM Khaidukov, and JC Krupa. Upconversion fluorescence of Er³⁺ trace impurity ions and Raman study in K₂YF₅: 0.1 mol% Tm³⁺ single crystal. *Journal of Alloys and Compounds*, 368(1-2):337–341, 2004.
- [9] VP Tuyen, VX Quang, NM Khaidukov, LD Thanh, NX Ca, N Van Hao, N Van Nghia, and P Van Do. K₂YF₅:Tb³⁺ single crystal: An in-depth study of spectroscopic properties, energy transfer and quantum cutting. *Optical Materials*, 106:109939, 2020.
- [10] M Yin, JC Krupa, E Antic-Fidancev, VN Makhov, and NM Khaidukov. Excitation spectroscopy of K₂YF₅: Pr³⁺ crystals. *Journal of Luminescence*, 101(1-2):79–85, 2003.
- [11] N Martin, R Mahiou, P Boutinaud, and JC Cousseins. A spectroscopic study of K₂YF₅:Pr³⁺. *Journal of Alloys and Compounds*, 323:303–307, 2001.
- [12] M Karbowiak, P Gnutek, and C Rudowicz. Energy levels and crystal field parameters for Nd³⁺ ions in BaY₂F₈, LiKYF₅, and K₂YF₅ single crystals. *Spectrochimica Acta Part A: Molecular and Biomolecular Spectroscopy*, 87:46–60, 2012.
- [13] M Yin, Y Li, N Dong, VN Makhov, NM Khaidukov, and JC Krupa. Spectroscopic studies and crystal field calculation for Nd³⁺ in single crystal K₂YF₅. *Journal of Alloys and Compounds*, 353(1-2):95–101, 2003.
- [14] KH Jang, ES Kim, L Shi, NM Khaidukov, and HJ Seo. Luminescence properties of Eu³⁺ ions in K₂YF₅ crystals. *Optical Materials*, 31(12):1819–1821, 2009.
- [15] P Boutinaud, R Mahiou, and JC Cousseins. Effect of one-dimensional structure on Tb³⁺ ⁵D₃–⁵D₄ cross-relaxation in K₂YF₅. *Journal of Luminescence*, 72:318–320, 1997.
- [16] PA Loiko, NM Khaidukov, J Méndez-Ramos, EV Vilejshikova, NA Skoptsov, and KV Yumashev. Up- and down-conversion emissions from Er³⁺ doped K₂YF₅ and K₂YbF₅ crystals. *Journal of Luminescence*, 170:1–7, 2016.
- [17] RE Peale, H Weidner, FG Anderson, and NM Khaidukov. Spectroscopy of Er³⁺ in K₂YF₅. *Advanced Solid State Lasers*, 10:462, 1997.
- [18] T Dean. Upconversion processes in Er³⁺ doped K₂YF₅. M.Sc. Thesis, University of Canterbury, 1998.
- [19] D Wang, Y Guo, Q Wang, Z Chang, J Liu, and J Luo. Judd–Ofelt analysis of spectroscopic properties of Tm³⁺ ions in K₂YF₅ crystal. *Journal of Alloys and Compounds*, 474(1-2):23–25, 2009.
- [20] Y Li, M Yin, N Dong, VN Makhov, NM Khaidukov, and JC Krupa. Spectra analysis of Tm³⁺ in K₂YF₅. *Journal of Physics and Chemistry of Solids*, 65(6):1059–1063, 2004.
- [21] SP Horvath, JPR Wells, MF Reid, M Honda, and M Yamaga. Electron paramagnetic resonance enhanced crystal-field analysis for low point group symmetry systems: C_{2v} sites in Sm³⁺:CaF₂/SrF₂. *Journal of Physics: Condensed Matter Physics*, 31:015501, 2019.

Spectroscopy of Er³⁺ in K₂YF₅

- [22] SP Horvath, JV Rakonjac, YH Chen, JJ Longdell, P Goldner, JPR Wells, and MF Reid. Extending phenomenological crystal-field methods to C₁ point group symmetry: characterization of the optically excited hyperfine structure of ¹⁶⁵Er³⁺:Y₂SiO₅. *Physical Review Letters*, 123:057401, 2019.
- [23] NL Jobbitt, SJ Patchett, Y Alizadeh, MF Reid, JPR Wells, SP Horvath, JJ Longdell, A Ferrier, and P Goldner. Transferability of crystal-field parameters for rare-earth ions in Y₂SiO₅ test by Zeeman spectroscopy. *Physics of the Solid State*, 61:780, 2019.
- [24] NL Jobbitt, JPR Wells, MF Reid, SP Horvath, P Goldner, and A Ferrier. Prediction of the optical polarization and high field hyperfine structure via a parametrized crystal-field model for the low symmetry centers in Er³⁺ doped Y₂SiO₅. *Physical Review B*, 104:155121, 2021.
- [25] G. W. Burdick and M. F. Reid. Crystal field parametrizations for low symmetry systems. *Mol. Phys.*, 102:1141–1147, 2004.
- [26] X Bian, Q Shi, L Wang, Y Tian, B Xu, ZK Mamybekov, P Huang, et al. Near-infrared luminescence and energy transfer mechanism in K₂YF₅:Nd³⁺, Yb³⁺. *Materials Research Bulletin*, 110:102–106, 2019.
- [27] M Ding, D Chen, Z Wan, Y Zhou, J Zhong, J Xi, and Z Ji. Hydrothermal synthesis of novel K₂YbF₅: Er³⁺/Y³⁺ microcrystals with tunable red–green upconversion luminescence. *Journal of Materials Science*, 50:6779–6785, 2015.
- [28] W T Carnall, G L Goodman, K Rajnak, and RS Rana. A systematic analysis of the spectra of the lanthanides doped into single crystal LaF₃. *The Journal of Chemical Physics*, 90(7):3443–3457, 1989.
- [29] Guokui Liu. Electronic Energy Level Structure. In G Liu and B Jacquier, editors, *Spectroscopic Properties of Rare Earths in Optical Materials*. Springer Science & Business Media, 2006.
- [30] MF Reid. Theory of rare-earth electronic structure and spectroscopy. In *Handbook on the Physics and Chemistry of Rare Earths*, volume 50, pages 47–64. Elsevier, 2016.
- [31] GH Dieke. *Spectra and Energy Levels of Rare-Earth Ions in Crystals*. Interscience Publishers, 1968.